Thermal Modeling of Rapid Single Flux Quantum Circuit Structures

Ana Mitrovic and Eby G. Friedman, *Fellow, IEEE*

***Abstract*—The operation of rapid single flux quantum (RSFQ) circuits depends upon the superconductive properties of the Josephson junctions (JJs) and metal layers, which are highly dependent on the temperature. Increasing densities and frequencies of JJs in RSFQ circuits have created a need to accurately model the local ambient thermal environment. In this article, an analytic thermal model of RSFQ circuit structures targeting the MIT Lincoln Laboratory SFQ5ee 10 kA/cm^2 technology is presented. The model is based on a network of thermal resistances, representing the heat generation and thermal paths within an RSFQ circuit. An error of less than 0.22% between the model and a numerical solver is achieved. To reduce the computational complexity, the sparsity of the matrix of thermal resistances among the nodes is increased by exploiting the effective radius of the heat spreading behavior. Ignoring the thermal effects of the heating elements outside of a target radius reduces the number of thermal resistances by 50%, increasing the maximum error of the model to only 0.26%.**

***Index Terms*—Single flux quantum (SFQ), superconducting integrated circuits, superconductive digital electronics, thermal analysis.**

I. Introduction

SINCE the introduction of rapid single flux quantum (RSFQ) in 1985, this technology has become the primary superconductive digital logic family [1]. The RSFQ logic family is based on Josephson junctions (JJs), exhibiting ultrahigh speed and ultralow power dissipation while operating at cryogenic temperatures. RSFQ circuits based on niobium are cooled below the boiling temperature of liquid helium, that is, 4.2 K.

The primary component of RSFQ circuits—the JJ—consists of two superconductive electrodes, typically composed of niobium and separated by a thin metal, insulator, or semiconductor barrier. Below 4.2 K, these junctions exhibit zero dc resistance, leading to the flow of supercurrent through the insulating barrier. Each JJ is characterized by a critical current I_C which, when exceeded, switches the junction into a resistive state, generating a voltage pulse across the JJ—a single flux quantum (SFQ) pulse. The operation of SFQ circuits is based on switching JJs between the superconductive state and resistive state and storing the SFQ pulses within inductive storage loops. The state of the logic cells is read by a clock signal, which switches the JJs and determines whether an SFQ pulse exists within the storage loop.

JJs are typically biased to approximately 0.7 of the critical current I_C. In RSFQ circuits, a bias current is provided by a resistive network. The static power, dissipated by the bias network, is the largest source of heat in RSFQ circuits.

Standard JJs exhibit hysteretic behavior, which is undesirable in RSFQ logic. These devices are therefore shunted with resistors to reduce this effect. During a switching event, the voltage pulse applied across these resistively shunted junctions (RSJs) dissipates power, mostly within the shunt resistor. A portion of the power is also dissipated in the barrier of the JJs due to the finite resistance exhibited in the normal state. The RSJs are therefore the primary source of dynamic power dissipation in SFQ circuits.

The critical current of a JJ also exhibits a temperature dependence, as shown in Fig. 1 [2]. Higher temperatures can lead to unwanted switching and incorrect logic behavior.

Recent progress in the design and fabrication of RSFQ systems has resulted in circuits operating at frequencies approaching 80 GHz and device densities exceeding 600 000 JJ/cm^2 [3]. Higher frequencies as well as an increasing number and density of junctions increase the ambient heat within these circuits. A model of the thermal behavior of SFQ circuits is therefore useful. In 1991, Lavine and Bai [2] developed an analytic model to analyze the thermal behavior of niobium nitride (NbN) JJs placed directly on a substrate in contact with a cryogen. In 2003, Ohki *et al.* [4] evaluated the heating characteristics of the bias resistor in a milliKelvin superconductive structure. A compact thermal model of SFQ circuit structures is not included in these models. Furthermore, since the introduction of these models, RSFQ fabrication technologies have evolved—some of the significant changes are in the number of metal layers, the composition of the materials, and properties of the resistors and JJs. In this article, the focus is on creating a tractable, analytic thermal model for RSFQ circuits in modern superconductive technologies.

An important SFQ fabrication technology is the SFQ5ee process developed at MIT Lincoln Laboratory [5], [6]. This technology includes eight niobium (Nb) layers and utilizes Nb/Al-AlOx/Nb JJs with a critical current density

Manuscript received January 19, 2022; revised March 7, 2022; accepted March 17, 2022. Date of publication April 12, 2022; date of current version April 22, 2022. This work was supported by the Department of Defense Agency Intelligence Advanced Research Projects Activity through the U.S. Army Research Office under Contract W911NF-17-9-0001. The review of this article was arranged by Editor J. Mateos. *(Corresponding author: Ana Mitrovic.)*

The authors are with the Department of Electrical and Computer Engineering, University of Rochester, Rochester, NY 14627 USA (e-mail: ana.mitrovic@rochester.edu; friedman@ece.rochester.edu).

Color versions of one or more figures in this article are available at https://doi.org/10.1109/TED.2022.3162172.

Digital Object Identifier 10.1109/TED.2022.3162172

0018-9383 © 2022 IEEE. Personal use is permitted, but republication/redistribution requires IEEE permission.
See https://www.ieee.org/publications/rights/index.html for more information.

Authorized licensed use limited to: UNIVERSITY OF ROCHESTER. Downloaded on May 23,2022 at 21:10:13 UTC from IEEE Xplore. Restrictions apply.

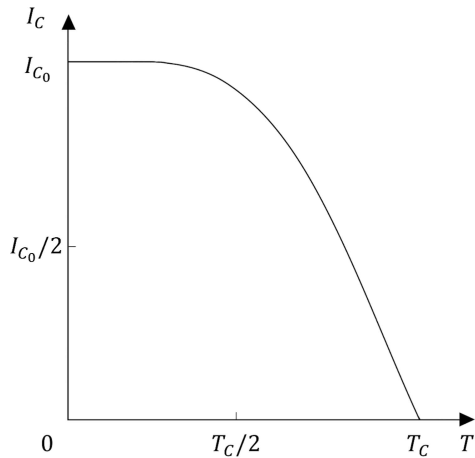

Fig. 1. Temperature dependence of the critical current of a JJ [2].

of $J_c = 100\ \mu\text{A}/\mu\text{m}^2$. In this article, an analytic thermal model for RSFQ circuit structures, targeting the SFQ5ee technology, is proposed. Validation of the model is performed using COMSOL Multiphysics[1] [7].

The article is organized as follows. In Section II, the thermal properties of materials used in SFQ circuits are described. In Section III, a thermal model of SFQ circuits is proposed. Validation of the model is described in Section IV. The article is concluded in Section V.

II. Material Properties at Cryogenic Temperatures

Heat conduction in a system is governed by the heat diffusion expression [7]

$$\rho c \frac{\partial T}{\partial t} = \nabla[\kappa \nabla T] + Q \tag{1}$$

where ρ represents the density of the material, c is the specific heat capacity, κ is the thermal conductivity, and the power density of the heat sources is represented by Q. To characterize the cooling behavior of SFQ integrated circuits, the convective boundary condition is used

$$\kappa \nabla T = h(T_{ext} - T) \tag{2}$$

where h represents the heat transfer coefficient, which describes the rate at which a circuit is cooled.

At cryogenic temperatures, the properties of the heat carriers—phonons and electrons—drastically change, greatly affecting the thermal properties of the materials [8]. Moreover, the transition of material into the superconductive state leads to the formation of Cooper pairs, degrading the ability of these materials to conduct heat [8]. Analyzing the thermal characteristics of SFQ circuits therefore requires understanding the thermal properties of materials at 4.2 K. The thermal conductivity, density, specific heat, and heat transfer coefficient are primary parameters, as noted in (1). These parameters exhibit a strong temperature dependence and behave differently when operating at cryogenic temperatures.

The metal layers and electrodes of the JJs are comprised of niobium. Other materials of interest are molybdenum (Mo), since the bias and shunt resistors are composed of this metal, SiO_2, which insulates the metal layers, and silicon (Si) that comprises the substrate. The thermal conductivity of these materials is described in Section II-A. The volumetric heat capacity depends upon the specific heat capacity and density of these materials. This parameter is reviewed in Section II-B. The thermal boundary resistance alters the heat paths within a circuit, changing the heat transfer coefficient. This parameter is discussed in Section II-C.

[1] Registered trademark.

TABLE I
Thermal Conductivity of Materials Used in Superconductive Integrated Circuits at 4.2 K

Material	Mo	Si	SiO_2	Nb
κ (W/m-K)	62	150	0.38	3.43

A. Thermal Conductivity

Heat is primarily conducted in solids by electrons and lattice waves, that is, the propagation of phonons. Thus, the total thermal conductivity can be described as [8]

$$\kappa = \kappa_e + \kappa_g \tag{3}$$

where κ_e is the electron component, and κ_g is the phonon component. In the superconductive state, most of the electrons are grouped into Cooper pairs, which do not contribute to the heat transport process [8]. For the thin superconductive films used in SFQ circuits, the mean free path of the phonons is short, leading to negligible κ_g [9]. The primary heat carriers in superconductive materials within SFQ circuits are therefore any remaining uncoupled electrons. The thermal conductivity within the normal state occurs above T_C which can be approximated using the Wiedemann–Franz law [9]

$$\kappa_{\text{nr}} = L_0 T \sigma_{\text{nr}} \tag{4}$$

where L_0 is the Lorenz number (2.45×10^{-8} WΩ/K^2), and σ_{nr} is the electrical conductivity within the normal state. From (4), the superconductive thermal conductivity can be estimated as [9], [10]

$$\kappa_s = \kappa_{\text{nr}} \frac{T}{T_C}. \tag{5}$$

For niobium, (5) has a value of ∼3.43 W/m-K at 4.2 K, consistent with other values reported in the literature [8], [10]. The wafer is comprised of high purity single-crystal silicon, whose thermal conductivity at 4.2 K is typically between 150 and 200 W/m-K [2], [11]. For Mo, κ ranges between 58.4 and 70.4 W/m-K [8], [12]. The thermal conductivity of SiO_2 ranges between 0.1 and 0.5 W/m-K [13], [14]. A typical value of the thermal conductivity of these materials is listed in Table I.

B. Volumetric Heat Capacity

At low temperatures, the contribution of lattice vibrations and thermal excitations of the electrons to specific heat can be described by

$$c = \gamma T + \beta T^3 \tag{6}$$

Authorized licensed use limited to: UNIVERSITY OF ROCHESTER. Downloaded on May 23,2022 at 21:10:13 UTC from IEEE Xplore. Restrictions apply.

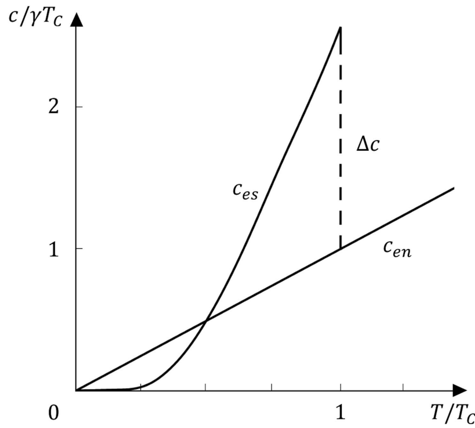

Fig. 2. Temperature dependence of the specific heat of superconductive materials. Note the difference between the superconductive electron specific heat c_{es} and normal electron specific heat c_{en} [14].

TABLE II
SPECIFIC HEAT AND DENSITY OF MATERIALS AT 4.2 K. THE DENSITY OF SiO_2 IS AT ROOM TEMPERATURE

Material	Mo	Si	SiO_2	Nb
$c\ \left(\frac{J}{kgK}\right)$	0.09 [16]	0.02 [16]	0.1 [13]	0.3 [12, 16]
$\rho\ \left(\frac{g}{cm^3}\right)$	10 [17]	2.33 [12]	2.2 (RT) [18]	8.61 [12]

where γ is a material related parameter describing the potential energy of the free electrons, and β describes the energy of the lattice vibrations within the material [14].

In the superconductive state, the specific heat of the electrons changes due to the formation of Cooper pairs, leading to a discontinuity at the critical temperature, described by [14]

$$\Delta c = 1.43\gamma T_C. \tag{7}$$

As shown in Fig. 2, below T_C, the superconductive electron specific heat c_{es} exponentially decreases at low temperatures [14]

$$c_{\text{es}} \sim e^{-\Delta/k_B T} \tag{8}$$

where Δ is the superconductive energy gap and k_B is the Boltzmann constant (1.38×10^{-23} J/K).

The specific heat and density of certain materials at 4.2 K are listed in Table II. Note that the values listed in Tables I and II are based on materials of different thicknesses than the materials used in SFQ circuits and may differ due to increased scattering of conduction electrons and lattice impurities [15].

C. Thermal Boundary Resistance

A primary issue in cooling superconductive circuits is the thermal boundary resistance, which appears at the boundary between two different materials due to the scattering of the heat carriers. Acoustic mismatch theory predicts this resistance to be [2], [4], [14]

$$R_{\text{thb}} = k_p/T^3. \tag{9}$$

For SFQ circuits operating at 4.2 K, the coefficient of proportionality k_p is approximately 10^{-3} m^2K^4/W, leading to the thermal boundary resistance R_{thb} which is approximately 10^{-5} m^2K/W [2], [19].

III. THERMAL MODEL

Several methods for modeling the thermal behavior of integrated circuits exist. The heat diffusion equation (1) can be solved numerically or analytically. Numerical methods exhibit high accuracy but produce large meshes, leading to high computational complexity. To reduce the complexity, a common approach for thermal modeling is based on analytic models of the thermal resistances and heat sources, creating a resistive mesh [20]. This approach is used in the RSFQ model presented here. The geometry used in this thermal model is described in Section III-A. Models of the heating and cooling characteristics are presented, respectively, in Sections III-B and III-C. The thermal model of an RSFQ circuit structure is described in Section III-D. Thermal coupling between each pair of heating elements is modeled by a resistance as part of a resistance matrix. The sparsity of this resistance matrix determines the computational complexity of the thermal model. The computational complexity and a method to increase the sparsity of the matrix are discussed in Section III-E. To validate the thermal model, COMSOL Multiphysics[1] simulation software, which utilizes the highly accurate 3-D finite-element method, is used.

A. Geometric Specifications

The thermal model is based on the specifications of the SFQ5ee fabrication technology, developed at MIT Lincoln Laboratory [5], [6]. This process includes eight superconductive niobium layers, each separated by an oxide layer on top of an oxidized Si substrate. The heating elements—bias resistors, JJs, and shunt resistors—are placed within the fifth metal and the oxide layer (respectively, layers M5 and O5), as shown in Fig. 3. Layer M6 is used for the inductors and interconnections among the logic elements. M1, M4, and M7 are the ground planes. The passive transmission lines and power lines are placed within the remaining metal layers—M0, M2, and M3 [6], [21].

A flip flop is used here to evaluate the thermal model. The D flip flop consists of six resistively shunted JJs and three bias current sources [21]. The structure is based on the SFQ5ee design rules with a 500 μm thick Si substrate.

B. Heating Properties

The heat flux of the bias resistor—the source of static power—can be evaluated using joule heating. Switching a JJ from the superconductive state into the normal state generates an SFQ pulse across the RSJ. To evaluate the heating behavior of resistively shunted JJs, the rms voltage across an RSJ is obtained. The resulting analytic expression for the heat flux sourced from a shunt resistor, based on joule heating, is

$$q_{\text{sh}} = \frac{{V_{\text{rms}}}^2}{R_{\text{sh}} A_{\text{sh}}} \tag{10}$$

Authorized licensed use limited to: UNIVERSITY OF ROCHESTER. Downloaded on May 23,2022 at 21:10:13 UTC from IEEE Xplore. Restrictions apply.

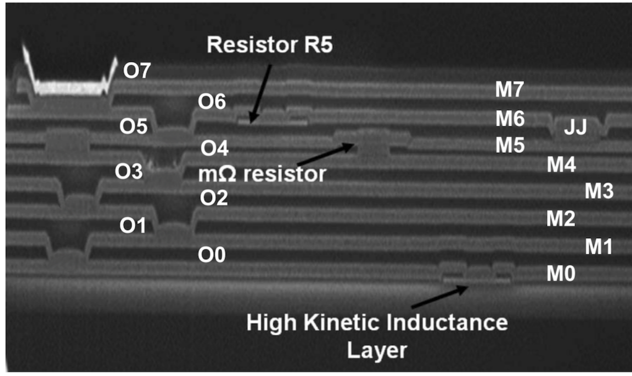

Fig. 3. Structure of the material layers used in the SFQ5ee technology [6], [22].

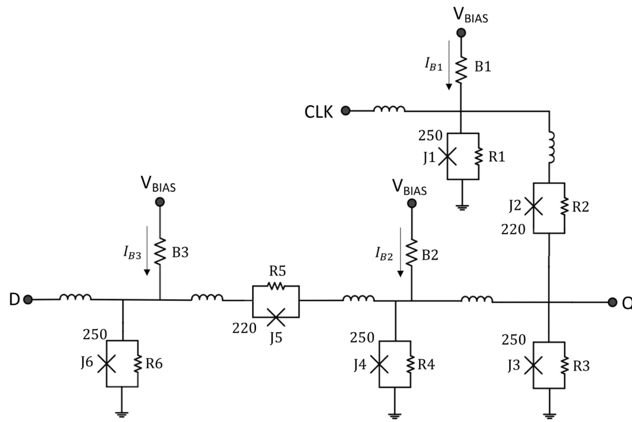

Fig. 4. D flip flop with heating elements—JJs (J), shunt resistors (R), and bias resistors (B). The element value placed next to the RSJs is the critical current of the JJ in μA [21], [23].

where the resistance of shunt resistor R_{sh} is evaluated assuming a critically damped JJ

$$R_{\text{sh}} = \sqrt{\frac{\Phi_0 J_C}{2\pi C_S}\frac{1}{I_C}} \tag{11}$$

where Φ_0 is the flux quantum ($\approx$2.07 mV·ps) and C_S is the specific capacitance of the junction (70 fF/μm^2 for the SFQ5ee process) [5], [19].

The heat flux due to heating a JJ is evaluated from the normal resistance of the junction, resulting in

$$q_{JJ} = \frac{{V_{\text{rms}}}^2 J_c}{V_{AB}}. \tag{12}$$

In (12), V_{AB} describes the relationship between the critical current and the normal resistance of a junction [22]

$$V_{AB} = I_C R_n. \tag{13}$$

The D flip flop, shown in Fig. 4, is assumed to operate at 50 GHz. The rms voltage for each RSJ is evaluated from SPICE simulations of this device [21], [23]. The circuit is evaluated based on the Whiteley Research/Synopsys JJ model, as described in [24].

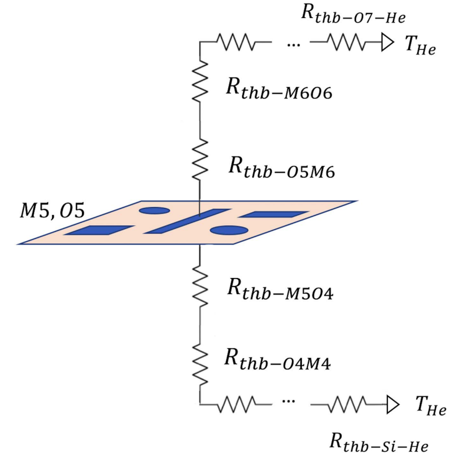

Fig. 5. Model of the thermal resistances comprising a vertical heat path.

C. Cooling Properties

Assuming the D flip flop is far from the boundary of an RSFQ integrated circuit, adiabatic boundary conditions can be applied to the lateral sides of the JTL structure. The primary heat path is therefore in the vertical direction. The heat travels from the heating elements within layers M5 and O5 through two vertical paths toward the helium bath. As shown in Fig. 5, these thermal paths can be approximated with a series network of resistors [2].

This network is comprised of thermal resistance for each material layer and an interfacial thermal resistance between each pair of layers. Due to the thin nature of these layers, however, the thermal resistance of the material layers is at least an order of magnitude smaller than the interfacial components and is therefore ignored [4]. The resulting model is a parallel network of two thermal boundary resistances. The inverse of the resulting resistance is the effective heat transfer coefficient h_{eff}. The interfacial thermal resistance between the metal layer M_i and the oxide layer O_j can be estimated based on the relative portion of metal M_{RP} within the material layers

$$R_{\text{thb}-M_i O_j} = M_{\text{RP}}(\%) \cdot R_{\text{thb}}. \tag{14}$$

D. Analytic Thermal Model

The analytic thermal model is based on a resistive mesh, as shown in Fig. 6 [20]. The current sources represent the power dissipated by each element. The thermal resistance of heating element x is

$$R_{\text{th}_x} = \frac{1}{\kappa_x}\frac{d_x}{A_x} \tag{15}$$

where κ_x is the thermal conductivity of the heating element material, A_x is the area of the element, and d_x is the thickness of the element. The convective cooling is modeled by a thermal resistance between the element and the cryogen

$$R_{\text{th}_{x-\text{He}}} = \frac{1}{h_{\text{eff}_x}}\frac{1}{\alpha_x A_x}. \tag{16}$$

In (16), h_{eff_x} is the effective heat transfer coefficient of the element, evaluated as described in Section III-C. Parameter α_x

Authorized licensed use limited to: UNIVERSITY OF ROCHESTER. Downloaded on May 23,2022 at 21:10:13 UTC from IEEE Xplore. Restrictions apply.

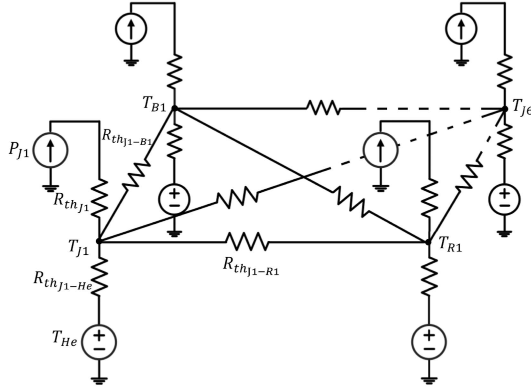

Fig. 6. Thermal model of SFQ circuit structure.

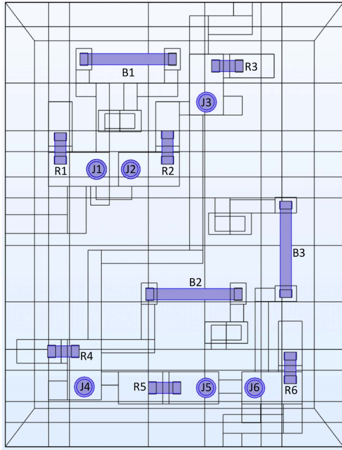

Fig. 7. Layout of D flip flop with highlighted heating elements—bias resistors and RSJs.

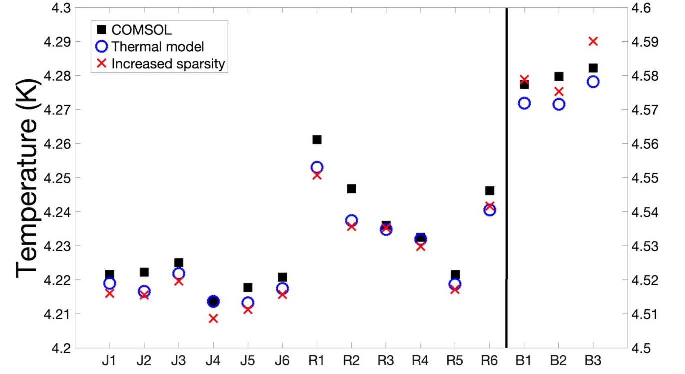

Fig. 8. Comparison of the analytic thermal model and COMSOL.

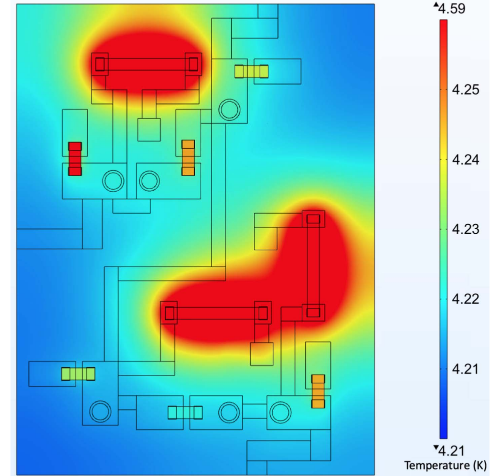

Fig. 9. Thermal profile of D flip flop simulated in COMSOL Multiphysics. For visibility, the color bar is limited to the range of 4.2 K to 4.26 K. The minimum and maximum temperatures are, respectively, shown at the bottom and top of the color bar.

describes the effective cooling area of the element caused by spreading the heat in the lateral directions [2]

$$\alpha_x = \left(1 + \frac{\eta_x}{r_x}\right)^2 \tag{17}$$

where r_x is the effective radius of the element [20], and η_x is the thermal healing length, which describes the effective radius of the heat spreading from the heat source [19]

$$\eta_x = \sqrt{\frac{\kappa_{\text{eff}_x} \cdot d_{\text{layer}}}{h_{\text{eff}_x}}}. \tag{18}$$

In (18), κ_{eff_x} is the effective thermal conductivity of the materials around the heating element, and d_{layer} is the thickness of the material layer within which the element is located.

The inter-node thermal resistance describes the thermal coupling between two heating elements. This thermal resistance consists of two parts. The two contributions to the thermal resistance are the thermal boundary resistance at the interface between the elements and the medium (19a), and an additional contribution due to the thermal resistance of the material between the heating elements (19b)

$$R_{\text{th1}_{x-y}} = \frac{R_{\text{thb}}}{A_x} + \frac{R_{\text{thb}}}{A_y} \tag{19a}$$

$$R_{\text{th2}_{x-y}} = \frac{1}{\kappa_{\text{mat}}} \frac{s_{x-y}}{\left(\frac{d_x+d_y}{2}\right) \cdot \max\left(w_x,\ w_y\right)}. \tag{19b}$$

In (19b), κ_{mat} is the thermal conductivity of the material conducting heat between elements x and y, approximated by the relative portion of the niobium within layers M5 and O5. d_x and d_y are, respectively, the thickness of elements x and y, w_x and w_y are, respectively, the width of elements x and y, and s_{x-y} is the distance between the elements.

E. Model Complexity

The number of thermal coupling resistances is described by

$$C_n^k = \frac{n!}{k!(n-k)!}. \tag{20}$$

From the above equation, this thermal model is applied to a D flip flop structure, resulting in 105 thermal coupling resistances between the JJs (J), shunt resistors (R), and bias resistors (B), which can be represented in a matrix form, as noted in (21), as shown at the bottom of the next page.

To increase the sparsity of the thermal coupling resistance matrix, the thermal coupling of each heating element is

Authorized licensed use limited to: UNIVERSITY OF ROCHESTER. Downloaded on May 23,2022 at 21:10:13 UTC from IEEE Xplore. Restrictions apply.

ignored for distances greater than the coupling radius [25]

$$r_c = -\ln\left(\frac{T_k}{R_{\text{th}}P - T_{\text{He}}}\right)\cdot\eta. \tag{22}$$

The sensitivity of the thermal model is described by the coefficient T_k in (22). Assuming $T_k = 1$ mK, the number of thermal coupling resistances is reduced to 37, significantly increasing the sparsity of the thermal resistance matrix, as noted in (23), as shown at the bottom of the page.

IV. Validation and Comparison

Based on the SFQ5ee design rules, the RSFQ D flip flop is evaluated by COMSOL Multiphysics. The layout of this D flip flop is shown in Fig. 7 [21]. The material parameters described in Section II are included in the COMSOL model, and the heating characteristics evaluated in SPICE are applied to the heating elements, as explained in Section III-B.

The thermal model is applied to the same structure. The results of the thermal simulation for different sparsities of the impedance matrix are shown in Fig. 8. For clarity, the values on the right vertical axis are attributed to the bias resistors. The thermal profile of the D flip flop, simulated in COMSOL, is shown in Fig. 9.

The relative difference between COMSOL and the thermal model is

$$\delta = \frac{|T_{\text{COMSOL}} - T_{\text{model}}|}{\text{average}(T_{\text{COMSOL}},\ T_{\text{model}})}. \tag{24}$$

$$M = \begin{bmatrix}
R_{J1J2} & R_{J1J3} & R_{J1J4} & R_{J1J5} & R_{J1J6} & R_{J1R1} & R_{J1R2} & R_{J1R3} & R_{J1R4} & R_{J1R5} & R_{J1R6} & R_{J1B1} & R_{J1B2} & R_{J1B3} \\
0 & R_{J2J3} & R_{J2J4} & R_{J2J5} & R_{J2J6} & R_{J2R1} & R_{J2R2} & R_{J2R3} & R_{J2R4} & R_{J2R5} & R_{J2R6} & R_{J2B1} & R_{J2B2} & R_{J2B3} \\
0 & 0 & R_{J3J4} & R_{J3J5} & R_{J3J6} & R_{J3R1} & R_{J3R2} & R_{J3R3} & R_{J3R4} & R_{J3R5} & R_{J3R6} & R_{J3B1} & R_{J3B2} & R_{J3B3} \\
0 & 0 & 0 & R_{J4J5} & R_{J4J6} & R_{J4R1} & R_{J4R2} & R_{J4R3} & R_{J4R4} & R_{J4R5} & R_{J4R6} & R_{J4B1} & R_{J4B2} & R_{J4B3} \\
0 & 0 & 0 & 0 & R_{J5J6} & R_{J5R1} & R_{J5R2} & R_{J5R3} & R_{J5R4} & R_{J5R5} & R_{J5R6} & R_{J5B1} & R_{J5B2} & R_{J5B3} \\
0 & 0 & 0 & 0 & 0 & R_{J6R1} & R_{J6R2} & R_{J6R3} & R_{J6R4} & R_{J6R5} & R_{J6R6} & R_{J6B1} & R_{J6B2} & R_{J6B3} \\
0 & 0 & 0 & 0 & 0 & 0 & R_{R1R2} & R_{R1R3} & R_{R1R4} & R_{R1R5} & R_{R1R6} & R_{R1B1} & R_{R1B2} & R_{R1B3} \\
0 & 0 & 0 & 0 & 0 & 0 & 0 & R_{R2R3} & R_{R2R4} & R_{R2R5} & R_{R2R6} & R_{R2B1} & R_{R2B2} & R_{R2B3} \\
0 & 0 & 0 & 0 & 0 & 0 & 0 & 0 & R_{R3R4} & R_{R3R5} & R_{R3R6} & R_{R3B1} & R_{R3B2} & R_{R3B3} \\
0 & 0 & 0 & 0 & 0 & 0 & 0 & 0 & 0 & R_{R4R5} & R_{R4R6} & R_{R4B1} & R_{R4B2} & R_{R4B3} \\
0 & 0 & 0 & 0 & 0 & 0 & 0 & 0 & 0 & 0 & R_{R5R6} & R_{R5B1} & R_{R5B2} & R_{R5B3} \\
0 & 0 & 0 & 0 & 0 & 0 & 0 & 0 & 0 & 0 & 0 & R_{R6B1} & R_{R6B2} & R_{R6B3} \\
0 & 0 & 0 & 0 & 0 & 0 & 0 & 0 & 0 & 0 & 0 & 0 & R_{B1R2} & R_{B1B3} \\
0 & 0 & 0 & 0 & 0 & 0 & 0 & 0 & 0 & 0 & 0 & 0 & 0 & R_{B2B3}
\end{bmatrix} \tag{21}$$

$$M_{\text{sparse}} = \begin{bmatrix}
R_{J1J2} & 0 & 0 & 0 & 0 & R_{J1R1} & R_{J1R2} & 0 & 0 & 0 & 0 & R_{J1B1} & R_{J1B2} & 0 \\
0 & 0 & 0 & 0 & 0 & R_{J2R1} & R_{J2R2} & 0 & 0 & 0 & 0 & R_{J2B1} & R_{J2B2} & 0 \\
0 & 0 & 0 & 0 & 0 & 0 & R_{J3R2} & R_{J3R3} & 0 & 0 & 0 & R_{J3B1} & 0 & R_{J3B3} \\
0 & 0 & 0 & 0 & 0 & 0 & 0 & 0 & R_{J4R4} & 0 & 0 & 0 & R_{J4B2} & 0 \\
0 & 0 & 0 & 0 & 0 & 0 & 0 & 0 & 0 & R_{J5R5} & R_{J5R6} & 0 & R_{J5B2} & R_{J5B3} \\
0 & 0 & 0 & 0 & 0 & 0 & 0 & 0 & 0 & 0 & R_{J6R6} & 0 & R_{J6B2} & R_{J6B3} \\
0 & 0 & 0 & 0 & 0 & 0 & 0 & 0 & 0 & 0 & 0 & R_{R1B1} & R_{R1B2} & 0 \\
0 & 0 & 0 & 0 & 0 & 0 & 0 & R_{R2R3} & 0 & 0 & 0 & R_{R2B1} & R_{R2B2} & R_{R2B3} \\
0 & 0 & 0 & 0 & 0 & 0 & 0 & 0 & 0 & 0 & 0 & R_{R3B1} & 0 & R_{R3B3} \\
0 & 0 & 0 & 0 & 0 & 0 & 0 & 0 & 0 & R_{R4R5} & 0 & 0 & R_{R4B2} & 0 \\
0 & 0 & 0 & 0 & 0 & 0 & 0 & 0 & 0 & 0 & 0 & 0 & R_{R5B2} & R_{R5B3} \\
0 & 0 & 0 & 0 & 0 & 0 & 0 & 0 & 0 & 0 & 0 & 0 & R_{R6B2} & R_{R6B3} \\
0 & 0 & 0 & 0 & 0 & 0 & 0 & 0 & 0 & 0 & 0 & 0 & 0 & 0 \\
0 & 0 & 0 & 0 & 0 & 0 & 0 & 0 & 0 & 0 & 0 & 0 & 0 & R_{B2B3}
\end{bmatrix} \tag{23}$$

Authorized licensed use limited to: UNIVERSITY OF ROCHESTER. Downloaded on May 23,2022 at 21:10:13 UTC from IEEE Xplore. Restrictions apply.

TABLE III
ACCURACY OF THERMAL MODEL WITH INCREASED SPARSITY. THE DIFFERENCES ARE THE DISCREPANCY BETWEEN COMSOL AND THE THERMAL MODEL

	Number of thermal resistances	$\|\Delta T\|_{average}$ (mK)	$\|\Delta T\|_{max}$ (mK)	$\delta_{average}$ (%)	δ_{max} (%)
Original sparsity	135	4.3	9.4	0.1	0.22
Increased sparsity (T_k=1 mK)	67	5.4	11	0.13	0.26

A comparison of the difference between the thermal model and the thermal model with greater sparsity, as described in Section III-E, is listed in Table III. Note that the greatest discrepancy between COMSOL and the thermal model is 11 mK (an error of 0.26%).

The maximum increase in temperature within a D flip flop is approximately 400 mK, as shown in Fig. 8. Although this increase does not compromise the operation of the D flip flop, it contributes to heating the cryogenic environment. This effect will significantly affect the operation of large scale RSFQ ICs. This thermal model of an RSFQ circuit structure can therefore be used as a step toward developing a thermal model for large scale RSFQ integrated systems as well as to analyze local hot spots within RSFQ ICs.

V. CONCLUSION

Due to increasing device densities and frequencies, thermal analysis is becoming an important part of the RSFQ circuit design process. To better understand the effects of heat generation and movement within a cryogenic environment, a model of the thermal behavior is important. An analytic thermal model of rapid SFQ circuit structures based on a thermal resistive mesh is presented in this article. To lower the computational complexity, the effective radius of the heat spreading behavior is exploited to increase the sparsity of the inter-node resistance matrix. Validation of the model is performed using COMSOL Multiphysics[1], resulting in a maximum discrepancy of 11 mK (an error of 0.26%) between the analytic model and COMSOL.

ACKNOWLEDGMENT

The content of the information does not necessarily reflect the position or the policy of the U.S. Government, and no official endorsement should be inferred.

REFERENCES

[1] G. Krylov and E. G. Friedman, *Single Flux Quantum Integrated Circuit Design*. Cham, Switzerland: Springer, 2022.

[2] A. S. Lavine and C. Bai, “An analysis of heat transfer in Josephson junction devices,” *J. Heat Transf.*, vol. 113, no. 3, pp. 535–543, Aug. 1991.

[3] T. Jabbari, G. Krylov, S. Whiteley, E. Mlinar, J. Kawa, and E. G. Friedman, “Interconnect routing for large-scale RSFQ circuits,” *IEEE Trans. Appl. Supercond.*, vol. 29, no. 5, pp. 1–5, Aug. 2019, doi: 10.1109/TASC.2019.2903023.

[4] T. A. Ohki, J. L. Habif, M. J. Feldman, and M. F. Bocko, “Thermal design of superconducting digital circuits for millikelvin operation,” *IEEE Trans. Appl. Supercond.*, vol. 13, no. 2, pp. 978–981, Jun. 2003, doi: 10.1109/TASC.2003.814118.

[5] S. K. Tolpygo, “Superconductor digital electronics: Scalability and energy efficiency issues,” *Low Temp. Phys.*, vol. 42, no. 5, pp. 361–379, May 2016, doi: 10.1063/1.4948618.

[6] S. K. Tolpygo *et al.*, “Advanced fabrication processes for superconductor electronics: Current status and new developments,” *IEEE Trans. Appl. Supercond.*, vol. 29, no. 5, pp. 1–13, Aug. 2019, doi: 10.1109/TASC.2019.2904919.

[7] *Heat Transfer Module User's Guide*, COMSOL Multiphysics v. 5.4. COMSOL AB, Stockholm, Sweden, 2018.

[8] Y. S. Touloukian, R. W. Powell, C. Y. Ho, and P. G. Klemens, *Thermal Conductivity-Metallic Elements and Alloys*. New York, NY, USA: Plenum, 1970.

[9] J. K. W. Yang, A. J. Kerman, E. A. Dauler, V. Anant, K. M. Rosfjord, and K. K. Berggren, “Modeling the electrical and thermal response of superconducting nanowire single-photon detectors,” *IEEE Trans. Appl. Supercond.*, vol. 17, no. 2, pp. 581–585, Jul. 2007, doi: 10.1109/TASC.2007.898660.

[10] A. Blois, S. Rozhko, L. Hao, J. C. Gallop, and E. J. Romans, “Heat propagation models for superconducting nanobridges at millikelvin temperatures,” *Superconductor Sci. Technol.*, vol. 30, no. 1, pp. 14003-1–14003-6, Nov. 2016.

[11] C. J. Glassbrenner and G. A. Slack, “Thermal conductivity of silicon and germanium from 3 K to the melting point,” *Phys. Rev.*, vol. 134, no. 4A, pp. A1058–A1069, May 1964, doi: 10.1103/PhysRev.134.A1058.

[12] J. E. Jensen, R. G. Stewart, W. A. Tuttle, and H. Brechna, *Brookhaven National Laboratory Selected Cryogenic Data Notebook*. Upton, NY, USA: Brookhaven National Laboratory, 1980.

[13] N. J. Simon, *Cryogenic Properties oflnorganic Insulation Materials for ITER Magnets: A Review*. Gaithersburg, MD, USA: National Institute of Standards and Technology, 1994.

[14] F. Pobell, *Matter Methods at Low Temperatures*, vol. 2. Berlin, Germany: Springer, 2007.

[15] P. Nath and K. L. Chopra, “Thermal conductivity of copper films,” *Thin Solid Films*, vol. 20, no. 1, pp. 53–62, Jan. 1974.

[16] Y. S. Touloukian, R. W. Powell, C. Y. Ho, and P. G. Klemens, *Specific Heat—Metallic Elements and Alloys*. New York, NY, USA: Plenum, 1970.

[17] C. A. Bryant and P. H. Keesom, “Low temperature specific heat of molybdenum,” *J. Chem. Phys.*, vol. 35, no. 3, pp. 1149–1150, Sep. 1961, doi: 10.1063/1.1701213.

[18] N. N. Greenwood and A. Earnshaw, *Chemistry of the Elements*. Amsterdam, The Netherlands: Elsevier, 2012.

[19] A. M. Kadin, C. A. Mancini, M. J. Feldman, and D. K. Brock, “Can RSFQ logic circuits be scaled to deep submicron junctions?” *IEEE Trans. Appl. Supercond.*, vol. 11, no. 1, pp. 1050–1055, Mar. 2001, doi: 10.1109/77.919528.

[20] W. Huang, M. R. Stan, K. Skadron, K. Sankaranarayanan, S. Ghosh, and S. Velusam, “Compact thermal modeling for temperature-aware design,” in *Proc. 41st Annu. Conf. Design Autom. (DAC)*, 2004, pp. 878–883, doi: 10.1145/996566.996800.

[21] S. S. Meher, C. Kanungo, A. Shukla, and A. Inamdar, “Parametric approach for routing power nets and passive transmission lines as part of digital cells,” *IEEE Trans. Appl. Supercond.*, vol. 29, no. 5, pp. 1–7, Aug. 2019, doi: 10.1109/TASC.2019.2899792.

[22] S. K. Tolpygo *et al.*, “Advanced fabrication processes for superconducting very large-scale integrated circuits,” *IEEE Trans. Appl. Supercond.*, vol. 26, no. 3, pp. 1–10, Apr. 2016, doi: 10.1109/TASC.2016.2519388.

[23] O. Brandel, O. Wetzstein, T. May, H. Toepfer, T. Ortlepp, and H. G. Meyer, “RSFQ electronics for controlling superconducting polarity switches,” *Superconductor Sci. Technol.*, vol. 25, Oct. 2012, Art. no. 125012, doi: 10.1088/0953-2048/25/12/125012.

[24] Whiteley Research Inc. *WRSPICE*. Accessed: Sep. 6, 2021. [Online]. Available: http://www.wrcad.com/wrspice.html

[25] J. Lee *et al.*, “Thermoelectric characterization and power generation using a silicon-on-insulator substrate,” *J. Microelectromech. Syst.*, vol. 21, no. 1, pp. 4–6, Feb. 2012, doi: 10.1109/JMEMS.2011.2175704.

Authorized licensed use limited to: UNIVERSITY OF ROCHESTER. Downloaded on May 23,2022 at 21:10:13 UTC from IEEE Xplore. Restrictions apply.